Cobalamin C Deficiency Shows a Rapidly Progressing Maculopathy With Severe Photoreceptor and Ganglion Cell Loss

Lucas Bonafede,[1] Can H. Ficicioglu,[2] Leona Serrano,[1] Grace Han,[1] Jessica I. W. Morgan,[1] Monte D. Mills,[3] Brian J. Forbes,[3] Stefanie L. Davidson,[3] Gil Binenbaum,[3] Paige B. Kaplan,[2] Charles W. Nichols,[1] Patrick Verloo,[4] Bart P. Leroy,[3,5,6] Albert M. Maguire,[1,3] and Tomas S. Aleman[1,3]

[1]Scheie Eye Institute and the Perelman Center for Advanced Medicine, Department of Ophthamology, Perelman School of Medicine at the University of Pennsylvania, Philadelphia, Pennsylvania, United States
[2]Department of Pediatrics, Section of Biochemical Genetics, The Children's Hospital of Philadelphia, Perelman School of Medicine at the University of Pennsylvania, Philadelphia, Pennsylvania, United States
[3]Division of Ophthalmology, The Children's Hospital of Philadelphia, Department of Ophthalmology, Perelman School of Medicine at the University of Pennsylvania, Philadelphia, Pennsylvania, United States
[4]Department of Pediatrics, Ghent University and Ghent University Hospital, Ghent, Belgium
[5]Department of Ophthalmology, Ghent University and Ghent University Hospital, Ghent, Belgium
[6]Center for Medical Genetics, Ghent University and Ghent University Hospital, Ghent, Belgium

Correspondence: Tomas S. Aleman, Perelman Center for Advanced Medicine, University of Pennsylvania, 3400 Civic Center Boulevard, Philadelphia, PA 19104, USA; aleman@mail.med.upenn.edu.

Submitted: August 2, 2015
Accepted: October 12, 2015

Citation: Bonafede L, Ficicioglu CH, Serrano L, et al. Cobalamin C deficiency shows a rapidly progressing maculopathy with severe photoreceptor and ganglion cell loss. *Invest Ophthalmol Vis Sci*. 2015;56:7875–7887. DOI:10.1167/iovs.15-17857

Purpose. To describe in detail the retinal structure and function of a group of patients with cobalamin C (cblC) disease.

Methods. Patients (n = 11, age 4 months to 15 years) with cblC disease (9/11, early onset) diagnosed by newborn screening underwent complete ophthalmic examinations, fundus photography, near-infrared reflectance imaging, and spectral-domain optical coherence tomography (SD-OCT). Electroretinograms (ERGs) were performed in a subset of patients.

Results. Patients carried homozygous or compound heterozygote mutations in the methylmalonic aciduria and homocystinuria type C (*MMACHC*) gene. Late-onset patients had a normal exam. All early-onset patients showed a maculopathy; older subjects had a retina-wide degeneration (n = 4; >7 years of age). In general, retinal changes were first observed before 1 year of age and progressed within months to a well-established maculopathy. Pseudocolobomas were documented in three patients. Measurable visual acuities ranged from 20/200 to 20/540. Nystagmus was present in 8/11 patients; 5/6 patients had normal ERGs; 1/6 had reduced rod-mediated responses. Spectral-domain OCT showed macular thinning, with severe ganglion cell layer (GCL) and outer nuclear layer (ONL) loss. Inner retinal thickening was observed in areas of total GCL/ONL loss. A normal lamination pattern in the peripapillary nasal retina was often seen despite severe central and/or retina-wide disease.

Conclusions. Patients with early-onset cblC and *MMACHC* mutations showed an early-onset, unusually fast-progressing maculopathy with severe central ONL and GCL loss. An abnormally thickened inner retina supports a remodeling response to both photoreceptor and ganglion cell degeneration and/or an interference with normal development in early-onset cblC.

Keywords: cobalamin C deficiency, optical coherence tomography, ganglion cells, pseudocoloboma, photoreceptors

Cobalamin C (cblC) disease is the most common inborn error of vitamin B12 metabolism with an estimated incidence of ~1:100,000 live births. Patients with this autosomal recessive disorder show homocysteinemia, homocystinuria, and methylmalonic aciduria and acidemia.[1–3] The disease is associated with neurologic, hematologic, ophthalmologic, cardiovascular, dermatologic, respiratory, and facial abnormalities and is subclassified as early onset, when presentation occurs before a year of age, and late onset, for patients presenting later in life.[1,4–9]

Mutations in the *MMACHC* (methylmalonic aciduria cblC type, with homocystinuria) gene, which encodes a protein involved in cobalamin cofactor synthesis, have been associated with cblC.[4,9–11] The ocular phenotype has been described through case reports, a handful of case series, and a single histopathologic report.[8,12–23] Ocular changes range from limited maculopathies to a progressive retina-wide degeneration and severe central vision loss. The exact mechanisms leading to the neurologic and/or ocular manifestations are currently unknown.

We recently reported the detailed spectral-domain (SD) optical coherence tomography (OCT) structural phenotype of a young patient with cblC. Retinal structure was characterized by photoreceptor and ganglion cell loss, the presence of a thickened surface layer, and a remodeled inner retina in regions of severe degeneration.[8] The maculopathy had developed from an initially normal retina into a well-stablished lesion within the first year of life, suggestive of interference with foveal development.[8]

To increase understanding of the visual dysfunction and retinal structural abnormalities resulting from cblC disease, we studied a group of patients with cblC disease and *MMACHC* mutations using measures of central vision, electrophysiology, and retinal structure. The results were compared to hereditary retinal degenerations with predominant macular involvement.

Methods

Eleven patients (ages 4 months to 15 years) diagnosed with early-onset cblC disease at the Children's Hospital of Philadelphia, University of Pennsylvania ($n = 10$), and at the Department of Ophthalmology, Ghent University, Belgium ($n = 1$), were included in this study. Patients were diagnosed as cblC through newborn metabolic screening and the diagnosis was confirmed by complementation assays and/or genotype. Subjects with normal vision ($n = 36$; ages 1–48 years) were also included. All patients underwent a comprehensive eye examination and best-corrected, age-appropriate, measurement of their central vision. Teller preferential looking cards or Snellen visual acuity provided quantitative measures of visual acuity in 8/11 patients. Data were collected retrospectively and included follow-up clinical exams encompassing up to 15 years, but did not include SD-OCT imaging; a shorter follow-up SD-OCT examination was available in one patient. Nonsedated (except for patient 1 [P1], age 4 months) SD-OCT imaging was performed using either a handheld capable system (iVue, Optovue, Inc., Fremont, CA, USA) with 6-mm-long sections, or with a desktop device (Spectralis, Heidelberg Engineering, Carlsbad, CA, USA) with 9-mm-long sections. High-resolution SD-OCT cross sections were performed across the fovea and through the optic nerve to have identifiable landmarks to compare with similar locations in normal subjects. The low-resolution (high-speed) setting of the Spectralis system was used whenever movement artifacts interfered with image acquisition. Segmentation of SD-OCT images was performed with the built-in segmentation software of the Spectralis and Optovue systems or with ImageJ imaging analysis software (http://imagej.nih.gov/ij/; provided in the public domain by the National Institutes of Health, Bethesda, MD, USA) supervised to ensure correct identification of the different laminar boundaries.[24] Standard full-field electroretinograms (ERGs) were recorded using a computer-based system (Espion; Diagnosys LLC, Littleton, MA, USA) in some ($n = 6$) of the patients.[25] Procedures adhered to the Declaration of Helsinki, and the study was approved by the institutional review boards of the participating institutions.

Results

Eleven unrelated patients with cblC carrying mutations in *MMACHC* participated in this study (Table). Six of the patients were from nonblack Hispanic families originally from Central America and Puerto Rico; the rest were Caucasian of European ancestry. There was no family history of ocular or metabolic disorders or of consanguinity. Most patients ($n = 8$) were examined during the first year of life after the diagnosis of cblC had been established. Nine patients showed some degree of developmental delay; brain magnetic resonance imaging showed abnormalities in 4/7 patients imaged (Supplementary Table S1). Biochemical abnormalities were aggressively treated and monitored from the time of diagnosis. Plasma methionine levels were maintained within normal range; some patients needed methionine supplementation. There was no obvious relationship between the degree of metabolic control and the severity of the ocular abnormalities (Supplementary Table S2). On their last exam, central vision was abnormal for the expected developmental age in all but one patient who had normal vision (P9); nystagmus was noted in most (8/11) patients (Table). The predominant refractive error was mild myopia, although the largest errors were hyperopic (Table). On their last visit, P3, P4, and P9 had normal retinal exams. Patient 3 had nystagmus with a normal-appearing retina (P3 and P4 did not have OCTs). The rest of the patients showed macular abnormalities at a young age. The central retinal appearance ranged from pigmentary changes to atrophic lesions (Fig. 1). The areas of atrophy showed a parafoveal distribution as a bull's-eye maculopathy or well-delimited central chorioretinal atrophy with (Fig. 1, P10; see also Fig. 3, P11), or without (Fig. 1, P5), posterior depression of the base of the lesion and the appearance of a pseudocoloboma (Table). A retina-wide pigmentary retinopathy was observed in older subjects (P7, P8, P10, and P11). The optic nerve appearance was normal in most patients; pallor or atrophy was noticed in 3/11 patients (Table). Electroretinograms were within normal limits in most (5/6) patients who had ERGs around presentation (P1, age 14 months; P3, 10 months; P5, 2 years; P7, 4 months; P8, 4 months; P10, 7 months); P7 had reduced amplitudes for rod-mediated responses and normal cone ERGs.

Early and Rapidly Progressive Photoreceptor and Ganglion Cell Degeneration

A horizontal SD-OCT cross section through the fovea in a normal subject showed the normal foveal contour and lamination of the retina (Fig. 2A). The three hyporeflective nuclear layers (outer nuclear layer [ONL]; inner nuclear layer [INL]; ganglion cell layer [GCL]) showed expected transitions in thickness with increasing eccentricity and were flanked by highly reflective bands corresponding to the retinal nerve fiber layer (RNFL) at the surface and two synaptic layers, the inner (IPL) and outer (OPL) plexiform layers. Outer retinal sublaminae are numbered in Figure 2A. A cross section in the patient examined at the youngest age (P1, age 4 months) demonstrated foveal thinning (114 μm) (normal mean ± 2 SD = 228 ± 30 μm).[26–29] The ONL and the GCL were less than half the normal thickness (Fig. 2A). Of note, the parafoveal region had no obvious signs of an impending bull's-eye maculopathy, such as increased backscattering posterior to the RPE. There was shortening of the outer segment and loss of the outer segment–RPE interdigitation signal in this region. The pattern contrasts with that observed in other maculopathies.[30–32] For example, a SD-OCT scan from a 9-year-old patient with Stargardt disease (STGD), the most frequent juvenile hereditary maculopathy, showed foveal ONL thinning (16 μm) exceeding that seen in P1 (54 μm; normal = 119 ± 39 μm), whereas the GCL at 0.6 mm of eccentricity in nasal retina, a region that receives input from foveal cones, was normal in the STGD patient (50 μm; normal = 34 ± 14 μm), but thin in P1 (12 μm), in the presence of less severe photoreceptor loss (Fig. 2A).[30] The RNFL was also abnormally thin (Fig. 2A), a finding that may be related to the loss of parafoveal GCL. A follow-up examination at 14 months of age revealed an unmistakable bull's-eye lesion (Fig. 2B).

Investigative Ophthalmology & Visual Science

Table. Clinical and Molecular Characteristic of the Patients

Pt #	Age at Exam/ Sex	Origin	Age at: Systemic Onset	Age at: Ocular Onset*	Age at: Last Normal Retinal Exam*	*MMACHC* Mutations Allele1/Allele2†	Visual Acuity (RE-LE)‡	Refraction‡	Fundus Exam§ Nystagmus	Fundus Exam§ Optic Nerve	Fundus Exam§ Macula	Fundus Exam§ Periphery	Foveal Thickness, µm OD	Foveal Thickness, µm OS
1	4 mo/F	Mexico	1 mo	9 mo	4 mo	c.352del/c.352del	CUSUM	−2.00	Y	p	nl	nl	na	127
2	9 mo/M	Puerto Rico	1 mo	12 mo	9 mo	c.430-2A>G/c.482C>T	20/360‖	−1.50	Y	nl	bem	nl	110	109
3	11 mo/F	United States	1 mo	8 mo	11 mo	c.271dupA/c.271dupA	20/380‖	−1.50	Y	nl	nl	nl	na	na
4	15 mo/M	Mexico	1 mo	n/a	15 mo	c.482G>A/c.609 G>A	20/540‖	−1.00	N	nl	nl	nl	na	na
5	2 y/F	Mexico	1 mo	8 mo	abn.	c.331C>T/c.615C>G	CSM	−1.00	N	nl	atrophy	nl	16	22
6	3 y/F	Guatemala	1 mo	na	abn.	c.328-331del/c.328-331del	FF	+1.50	Y	nl	atrophy	nl	na	na
7	7 y/M	United States	1 mo	5 mo	3 mo	468delCT/440C>A	20/250	−1.75	Y	nl	bem	pigm.	88	93
8	8 y/M	Belgium	3 wk	4 mo	abn.	c.271-272dupA/c.271-272dupA	20/320	+2.25	Y	nl	bem	pigm.	na	na
9	9 y/F	Mexico	1 mo	n/a	9 y	c.328/331del/c.566G>A	20/25	−3.00	N	nl	nl	nl	220	224
10	13 y/M	United States	1 wk	9 mo	3 mo	c.271-272dup A/c.271-272dup A	20/400	+5.50	Y	p	p-coloboma	pigm.	52‖	na
11	15 y/M	United States	1 mo	na	abn.	c.271-272dupA/c.500delC	20/400	−1.00	Y	a	p-coloboma	pigm.	na	45‖

Age given in months or years at age of first exam or OCT; age of systemic onset coincides with age at diagnosis; onset at 1 m refers to diagnosis ≤ 1 month of age; P10 has been reported previously.[8] na, not available; n/a, nonapplicable; nl, normal; Y, yes; N, no; abn., abnormal at initial visit with us; CUSUM, central, unsteady, unmaintained; CSM, central, steady, maintained; FF, fixates and follows; p, pallor; pigm., pigmentary change (includes mottling, depigmentation); bem, bull's-eye maculopathy; p-coloboma, pseudocoloboma.

* Ocular onset, earliest documented ocular abnormality/nystagmus; no earlier exam or record.

† Predicted amino acid change; diagnosis confirmed by complementation assay.

‡ Visual acuity and refraction (spherical equivalent), similar in both eyes, unless specified.

§ Visual acuity measured binocularly by preferential looking with Teller visual acuity cards.

‖ Thickness of remnant tissue at the center of the pseudocoloboma.

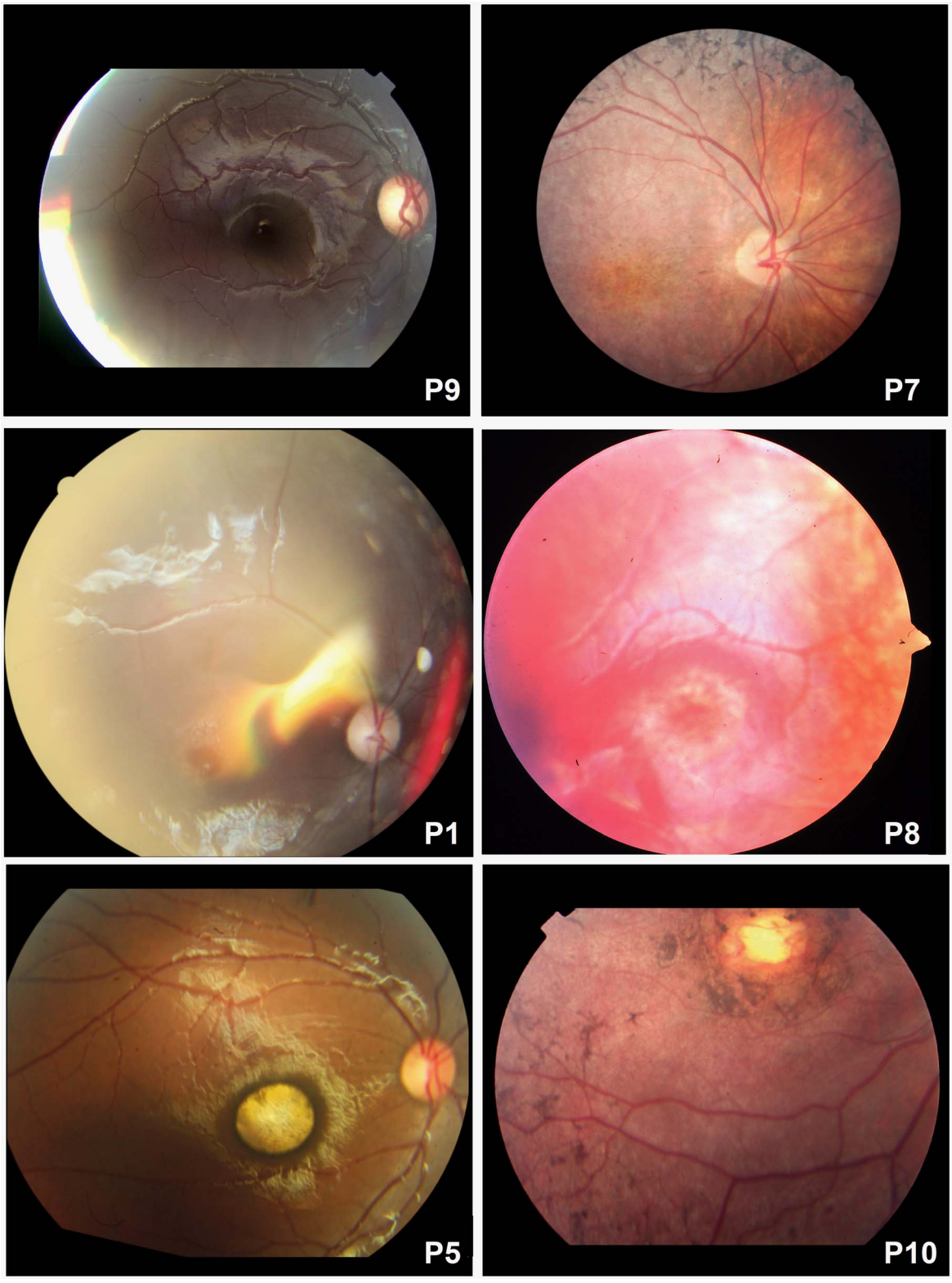

Figure 1. Fundus images demonstrating spectrum of findings.

Spectral-domain OCT through this region showed a transition from a well-laminated retina to a zone of ONL and GCL thinning (Fig. 2B, arrow) accompanied by increased backscattering (Fig. 2B, bracket) posterior to the RPE, which was not present in the scans at age 4 months. The GCL in this region turned into a poorly laminated layer with intervening hyperreflectivity. In total, four patients (P1, P2, P7, P10) had an initial normal retinal exam and developed a rapidly

Investigative Ophthalmology & Visual Science

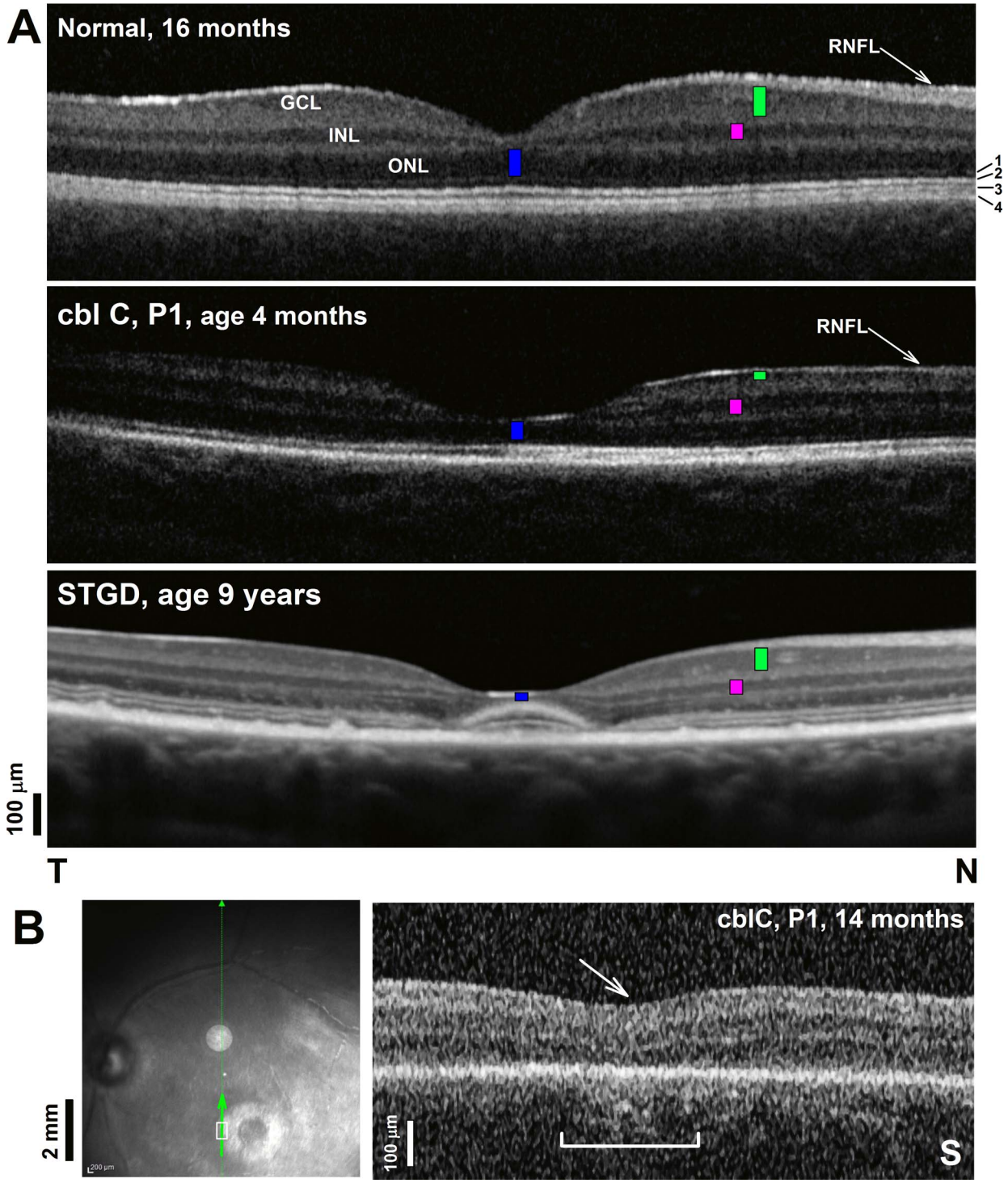

Figure 2. Earliest abnormalities and fast progression of early cblC-associated retinal degeneration. (**A**) Shown are 6-mm-long horizontal SD-OCT cross sections through the fovea in a normal subject compared with a 4-month-old cblC patient (P1). Nuclear layers and the retinal nerve fiber layer (RNFL) are labeled. *Color bars* are overlaid on each nuclear layer (ONL, *blue*; INL, *pink*; GCL, *green*) to facilitate comparisons. *INL* and *GCL bars* are positioned at a location in the parafovea that receives input from foveal cones. Outer photoreceptor/RPE sublaminae are labeled to the *right* following nomenclature recently proposed[24]: 1, outer limiting membrane; 2, ellipsoid region; 3 interdigitation between photoreceptor outer segment tips and RPE cells; 4, RPE. A 9-year-old patient with Stargardt disease (STGD) and more severe foveal thinning but preserved inner retina is shown for comparison. (**B**) Near-infrared reflectance (NIR-REF) image (*left*) of the same patient (P1) at 14 months of age showing a bull's-eye maculopathy; round image superonasal to the fovea is a reflection artifact. *Green arrow* indicates direction of the SD-OCT scan; *box* encloses region magnified at *right*. The cross section through the parafoveal region shows a transition zone from a well-laminated retina to a region with ONL and GCL thinning (*bracketed*) and increased posterior backscattering (*arrow*).

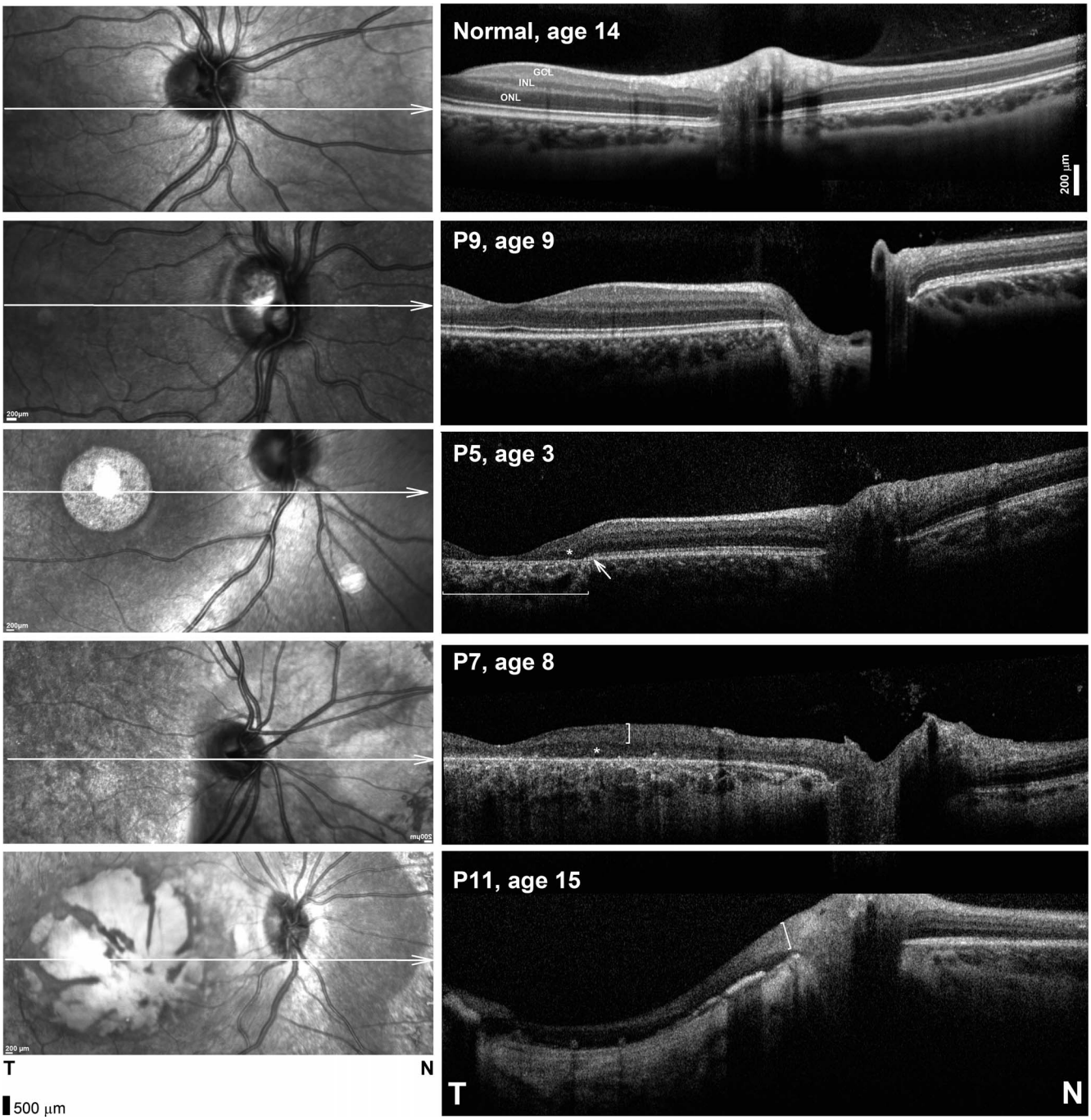

FIGURE 3. Spectrum of structural abnormalities in early cblC-associated retinal degeneration. *Left*: NIR-REF images are shown to illustrate the appearance of the central abnormalities and the nasal peripapillary preservation (P7 and P11). *Overlaid white arrow* denotes the direction and region scanned with SD-OCT. All images portrayed as right eyes. *Calibration bar* at *bottom left. Right*: horizontal, 9-mm-long SD-OCT cross sections in four patients illustrating the spectrum of structural abnormalities encountered. Nuclear layers are labeled in the normal subject as in Figure 2; *calibration bar* is to the *bottom right. Arrow* (P5) points to the region of steep transition in retinal structure. *Horizontal bracket* (P5) delimits region of increased posterior backscatter. *Vertical brackets* (P7 and P11) delimit thick hyperreflective superficial layer that exceeds thickness of the normal RNFL for the respective location. *Asterisk* denotes delaminated retina with amalgamation of the INL and the ONL. Images shown as right eyes but were similar in each eye of every patient. *Calibration bar*: *bottom left*. T, temporal; N, nasal.

progressing maculopathy between 5 and 14 months of age, an unusually fast progression compared to other hereditary maculopathies (Table).[8,22,33] Other patients (P5, P6, P8, P11) were abnormal at presentation between 4 and 8 months of age; earlier exams did not take place or there were no records available to determine if their retinas were normal earlier (Table).

Macular Changes in cblC-Associated Retinal Degeneration

Foveal thinning was observed in all patients examined with OCT, except P9 (Table). Horizontal SD-OCT scans extending from the fovea into the optic nerve illustrate the spectrum of abnormalities encountered (Fig. 3). Images from P10 have been

published previously.[8] Retinal structure was within normal limits in one patient (P9). On near-infrared reflectance imaging, a well-demarcated, round foveal lesion in P5 was associated with severe retinal thinning and posterior backscattering (Fig. 3, bracket). The inner retina appeared disorganized just eccentric to the foveal center with amalgamation of remnants of the ONL and INL leading to a thick hyporreflective band (Fig. 3, asterisk). The INL and GCL were discernible ~600 μm from the foveal center, where there was a steep transition (Fig. 3, arrow) to a normally laminated retina. The order in which each one of the outer retinal layers became visible with eccentricity was ONL, outer segment (OS)-RPE interdigitation, inner segment (IS)/OS, and the external limiting membrane (ELM). At this location the GCL appeared slightly thinner compared to normal. More extensive abnormalities were exemplified by two other patients. On NIR-REF the central retina of P7 was not homogeneous in appearance (Fig. 3). The fovea was thin with a flattened foveal contour, likely a consequence of GCL thinning and loss of the foveal ridge.[34] The ONL and GCL could not be discerned. There was a broad hyporeflective band in the outer retina, likely an INL-ONL amalgamate (Fig. 3, asterisk), and a thickened highly reflective superficial band that included the IPL (Fig. 3, vertical bracket). Near the temporal edge of the optic nerve, a thin ONL was again visible with a poorly defined GCL; the ELM, IS/OS, OS-RPE interdigitation were not discernible. At a greater eccentricity, nasal to the optic nerve, the retina returned to a near normal lamination pattern. On NIR-REF imaging, P11 showed a large central hyporeflective lesion with the appearance of a pseudocoloboma, reminiscent of published images from P10.[8] Around this central atrophy there was an annular area of pigmentary change; just peripheral to the vascular arcades there was bone spicule pigmentation (not shown). A thin ONL and INL were visible only near the temporal margin of the optic nerve; the GCL was not discernible throughout the central retina. There were intraretinal hyperreflectivities within the central lesion that represent RPE hypertrophy and migration. There was a thick hyperreflective surface band toward the temporal edge of the optic nerve that resembled the appearance of P10 (Fig. 3, vertical bracket).[8] The retina nasal to the optic nerve was remarkably well preserved and colocalized, as in P7, with darker islands of peripapillary RPE preservation on NIR-REF (Fig. 3).

Early Retinal Changes in cblC-Associated Retinal Degeneration

Cross-sectional SD-OCT images along the vertical meridian in two patients (P1 and P2) representing the earliest disease stages were compared to a normal subject (Fig. 4). The normal retina showed a well-defined foveal depression; the GCL was thickest at ~1 mm of eccentricity, contributing to the shape of the foveal ridge.[34] Both patients showed central retinal thinning that was less severe with increasing eccentricity and a bull's-eye maculopathy on NIR-REF (Fig. 2, P1; P2 not shown). The nuclear layers were identifiable throughout the extent of the scans in both patients; the GCL and ONL were thinner than normal with a flattened foveal contour caused by a thinned GCL (Fig. 4, arrows). The RNFL in P1 appeared slightly thinner than normal. Quantitation of the images confirmed more prominent central changes (Fig. 4B). The total retina was abnormally thin throughout the extent of the scans, especially within 3 mm of the fovea. The RNFL was slightly reduced in thickness centrally, but returned to within normal limits with increasing eccentricity. The GCL from 0.6 to 1 mm of eccentricity was less than 25% of the normal thickness. With increasing eccentricity the GCL approaches normality. At most central (<3 mm) locations, the INL was within normal limits or slightly thicker than normal (data not shown). There were no localized changes in GCL+IPL thickness in regions of GCL loss, which suggests replacement of ganglion cells by nonneuronal elements. Foveal ONL thickness was reduced to ~50% of normal and returned to normal limits at approximately 4 mm from the center.

Intraretinal Variation in Structure and Retinal Remodeling in Early-Onset cblC

Near-infrared REF imaging in P8 showed a darker peripapillary island of RPE preservation surrounded by depigmented retina similar to what was seen in other patients (Figs. 3, 5A). A horizontal SD-OCT scan through this region showed relative preservation of the retinal architecture, particularly on the nasal side. There was a thin ONL and GCL temporal to the nerve, which became undetectable at greater distances from its margin. Nasal to the nerve there was a deceptively normal lamination and normal-appearing ONL and INL. The GCL at this location was barely detectable, and there was a thick highly reflective band that extended from the retinal surface to the IPL. Farther into nasal retina was gradual thinning of the ONL and the GCL. The ONL and GCL became undetectable and the retina acquired a bilaminar appearance with an outer hyporeflective band and a thicker inner hyperreflective band (Fig. 5A, arrow) with intraretinal hyperreflectivities (Fig. 5A, asterisk).

Magnified sections from a region ~1 mm temporal and nasal to the optic nerve were examined to determine the relationships between the abnormalities observed for each of the layers across different patients (Fig. 5B). The peripapillary retina showed a normal-appearing retinal structure in P9 and P5. Sections from the temporal peripapillary retina in P10 and P8 showed ONL and GCL thinning with relative preservation of the INL (Fig. 5B, top). The GCL in these patients was barely perceptible within a thick superficial hyperreflective layer. Outer retinal structures such as the ELM can be seen in P8 despite the severity of the degeneration (Fig. 5B, asterisk). Patient 7 and P11 illustrated more severe disease with disorganized retinas. Patient 11 had a bilaminar retinal appearance likely representing inner retinal remodeling with replacement of ganglion cells by nonneuronal elements and amalgamation of the INL and ONL, respectively. Sections from the nasal peripapillary retina showed normal-appearing ONL and INL in all patients (Fig. 5B, bottom). The GCL could be normal in thickness but had ill-defined boundaries (Fig. 5B, P5 and P8). There was variable thickening of the retina vitread to the GCL.

Spectral-domain OCT cross sections were quantified to better understand the structural abnormalities (Fig. 5C). Included were two central locations (fovea and 1 mm of eccentricity, $n = 7$ patients), where photoreceptor and ganglion cell contributions to the nuclear layer thicknesses in normal retinas are expected to be maximal, and peripapillary locations (3 and 7 mm nasal to the fovea, $n = 6$ patients), regions with relative preservation of the retinal architecture in cblC. Measurements for each retinal layer are expressed as a percentage of the mean normal for each retinal region. For the central locations, inner retinal measurements (GCL, GCL+IPL, INL) were performed in regions laterally displaced by 0.6 mm in relationship to the foveal photoreceptors they receive input from.[35] For the central locations, all patients (except P9) showed foveal thinning with severe ONL, GCL, and RNFL loss. Patient 9, who had a normal SD-OCT appearance, had a mildly thin GCL and RNFL but normal ONL and INL. Less severe GCL and ONL loss was observed at 1 mm from the foveal center in all patients. At both eccentricities there was INL preservation in most (P1, P3, P5, P9) patients. Thickening of the INL (P7 and P10) and of the RNFL (P10) was associated with severe ONL

Investigative Ophthalmology & Visual Science

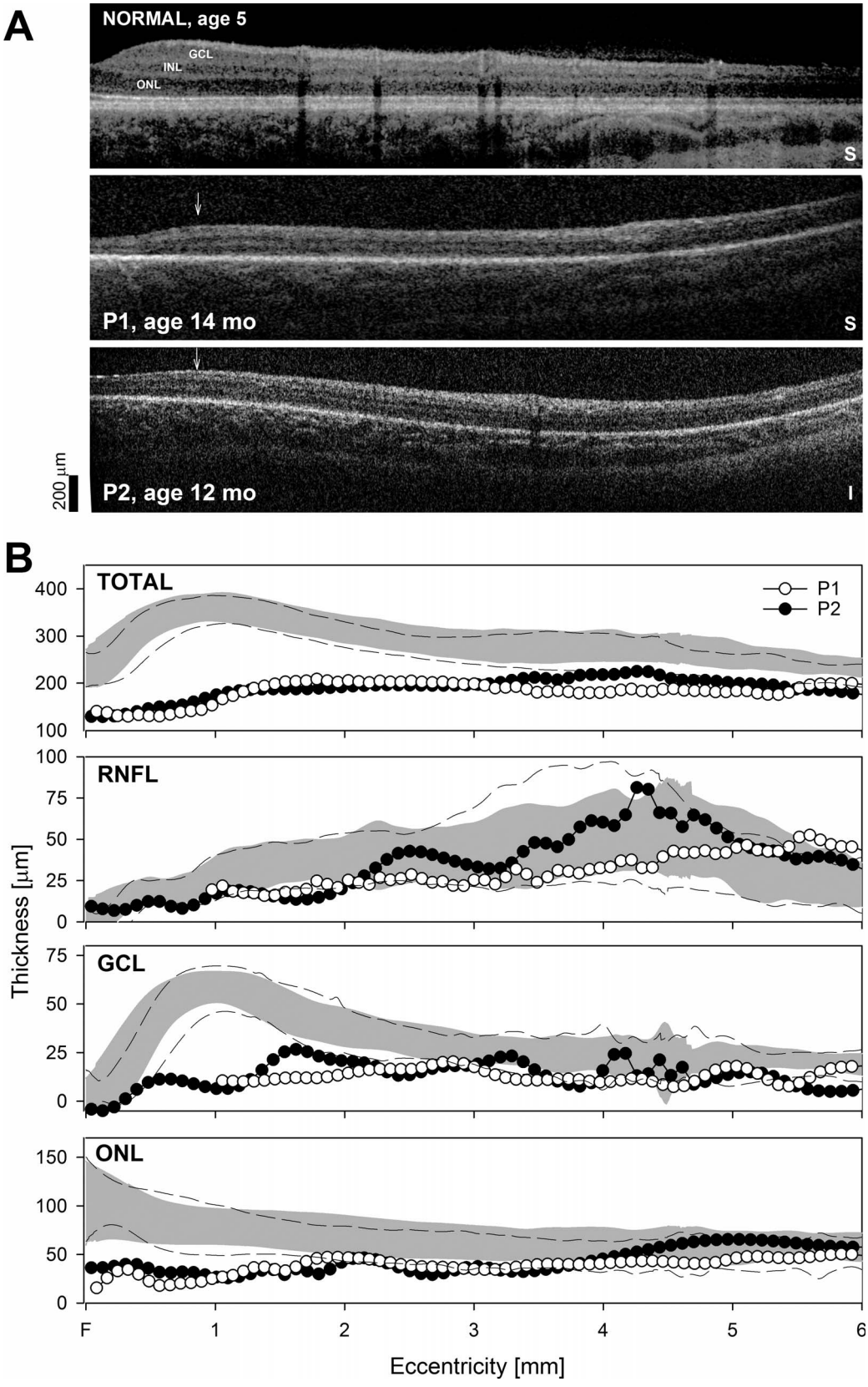

Figure 4. Detail of the initial abnormalities in early-onset cblC disease-associated maculopathy. (**A**) Nine-millimeter-long nonstraightened SD-OCT cross sections along the vertical meridian from the fovea in a normal subject (*top*) compared with two patients with the earliest abnormalities (*below*) in cblC disease. Severe ONL thinning and a flattened foveal contour that results from GCL loss (*arrows*) are shown. Nuclear layers are labeled in the normal subject as in Figure 2. S, superior retina; I, inferior retina. *Calibration bar* to the *bottom left*. (**B**) Overall retinal, RNFL, GCL, and ONL thicknesses along the vertical meridian in both patients. *Shaded bands*: normal limits for vertical superior retina (mean ± 2 SD; $n = 26$, age range, 11–49); normal limits for inferior retina are very similar (*dashed lines*).

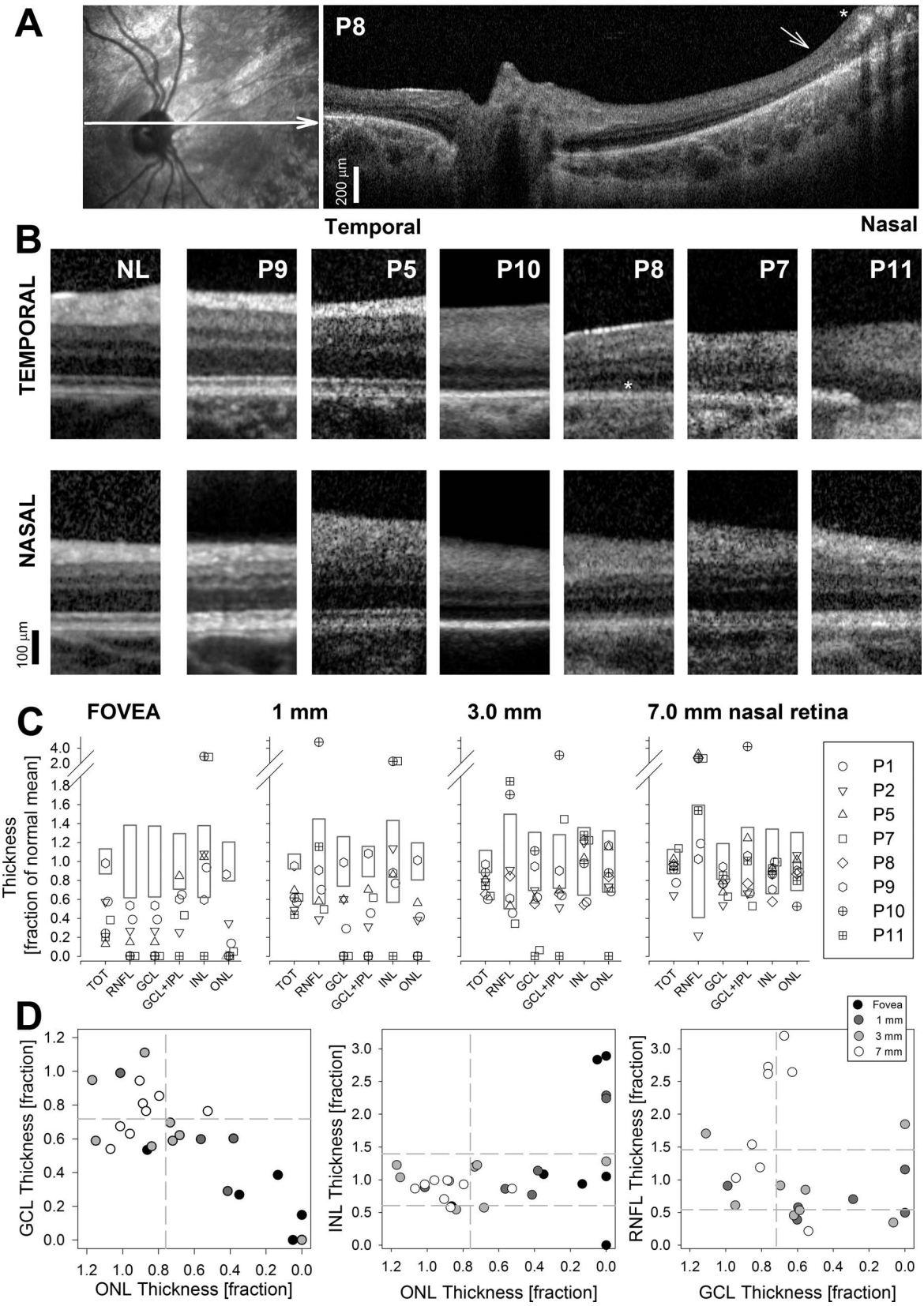

Figure 5. (**A**) Intraretinal variation in disease expression in cblC-associated retinal degeneration. Near-infrared reflectance imaging (*left*) of the optic nerve and peripapillary retina in a representative patient; *overlaid white line* defines region scanned with SD-OCT. Horizontal 9-mm-long SD-OCT cross section through the optic nerve head extending from the temporal peripapillary region into nasal retina demonstrating relative preservation of the nasal peripapillary retinal structure (*right*). *Vertical arrow* denotes transition to a region of remodeled, thickened retina. (**B**) Magnified SD-OCT cross sections from regions located 1 mm from the optic nerve in temporal (*top*) and nasal (*bottom*) peripapillary retina. Scans are aligned by the RPE layer. (**C**) Quantitation of structural changes in cblC patients. Plots of thickness for main retinal layers at two central (fovea

and 1 mm of eccentricity, $n = 7$ patients) and peripapillary locations (3 and 7 mm nasal to the fovea, $n = 6$), regions with relative preservation of the retinal architecture. Measurements for each retinal layer are expressed as a percentage of the mean normal for each retinal region. For the central locations, inner retinal measurements (GCL, GCL+IPL, INL) were performed in regions laterally displaced in relationship to the foveal photoreceptors (ONL) they receive input from.[35] *Boxes* define the normal range (mean ± 2 SD; $n = 35$, age range, 10–49). (**D**) Photoreceptor to ganglion cell and INL relationships in patients. Ganglion cell layer and INL thickness as a function of ONL thickness (*left* and *center*) and RNFL thickness as a function of RNFL thickness (*right*). Thicknesses as expressed as a fraction of the mean normal value at each retinal location. Ganglion cell layer and INL measurements for central locations are laterally displaced as in (**C**). *Dashed lines*: normal limits (horizontal: ± 2 SD from normal mean thickness; vertical: −2 SD of normal mean thickness). *Symbols* distinguish the different eccentricities explored.

loss suggestive of inner retinal remodeling.[36–39] For the peripapillary locations, there was relative preservation of the ONL and INL; GCL thickness in this region was within normal limits or thin. The RNFL was thicker than the normal mean in all but one patient (P2).

Next, the interrelationships between the changes observed in each of the main retinal layers were explored by plotting thickness expressed as the fraction of the normal mean at the corresponding retinal locations for each layer, laterally displaced, as described (Fig. 5D). There was a nearly proportional thinning of both the ONL and GCL for most of the range of thicknesses measured. A notable abnormality was the observation of GCL loss in locations with normal ONL thickness, suggesting greater susceptibility of the GCL to damage (Fig. 5D, left graph). The INL was within normal limits for most locations across a wide range of ONL values, with thickening observed only at the most central, severely affected loci (Fig. 5D, middle). The relationship between the RNFL and the GCL thickness was less clear (Fig. 5D, right graph). The RNFL was within normal limits or thick for most loci, with only a mild tendency toward thinning at the most central locations with severe GCL and ONL loss. The RNFL was thick in locations with mild GCL thinning in nasal peripapillary retina.

Discussion

Early-Onset, Fast-Progressing Photoreceptor and Ganglion Cell Degeneration

Early retinal changes in this cohort of patients with early-onset, *MMACHC*-positive cblC included foveal thinning, likely from cone photoreceptor loss, and profound parafoveal GCL loss. There were retina-wide abnormalities likely representing involvement of all photoreceptor subtypes. Photoreceptor outer segment loss and ONL thinning were the earliest changes in the outer retina. Inner retinal findings included a relatively spared INL in locations with obvious ONL and GCL loss, amalgamation of the INL and ONL in central regions with severe ONL loss, GCL thinning with approximation of the IPL to the RNFL, and the presence of a highly reflective thickened superficial layer in place of the RNFL. There was no obvious relationship between the genotype and the severity of the SD-OCT abnormalities, although meaningful gradation of the structural abnormalities within this small cross-sectional sample was not possible. There was a normal retinal structure in P9 and normal fundus appearance in P4 (with presumed subnormal visual acuity). Both patients reached normal developmental milestones and had mild metabolic abnormalities. It is possible that newborn metabolic screening may have led to the detection of a presymptomatic phenotype in these patients. Long-term follow-up will help clarify this possibility. Patient 3, who carried a homozygote mutation known to cause early-onset cblC, had nystagmus but a normal retinal exam and ERGs at ∼11 months of age; OCT was not available. The current work demonstrated subclinical retinal disease in cblC, a possibility in this patient.

Several patients showed an early-onset, fast-progressing maculopathy evolving during the first 2 years of life, confirming previous observations.[14,15,18,19,22] The changes occur during a critical stage of foveal postnatal development and visual maturation and raise the possibility of a particular vulnerability of the central photoreceptors and/or ganglion cells to the metabolic abnormality during this period.[8,16,22,40] The magnitude of the abnormalities, particularly at the level of the GCL, exceeded the changes expected to occur due to normal foveal development.[28] A nonsyndromic bull's-eye maculopathy reported in an adult patient who was subsequently diagnosed as having *MMACHC*-positive cblC disease did not show GCL loss in the presence of severe foveal thinning, suggesting less vulnerability later in life.[21] Such fast progression and GCL abnormalities have not been described in other maculopathies, such as STGD and forms of cone-rod dystrophy.[30–33] That is, central primary photoreceptor disease is not typically accompanied by GCL loss; instead, the central GCL shows minimal change or is thickened, and when GCL loss is observed it is in association with severe photoreceptor loss.[30,32,41] In contrast, there was equal or greater GCL compared to ONL thinning in early-onset cblC arguing in favor of a central role of the ganglion cell abnormality in the pathophysiology. The findings also recapitulate the only detailed ocular histopathologic report available for this condition.[23]

Regional Variation in Disease Severity in cblC-Associated Retinal Degeneration

A spectrum of central disease severity ranging from bull's-eye maculopathies to foveal chorioretinal atrophy has been reported in cblC and was observed in our patients (reviewed in Refs. 8, 22). Severe disease was characterized by foveal atrophy with the appearance of macular pseudocolobomas, which have been described in early-onset cblC disease as well as in conditions in the spectrum of Leber's congenital amaurosis, suggesting that these lesions may not be necessarily congenital but the result of fast-progressing, severe foveal disease occurring during a critical early postnatal period.[8,40,42,43] One gene is now known to be consistently associated with this type of lesion, suggesting a common mechanism that may be shared by cblC.[42–49] It is noteworthy that the central retinal structure in patients with early ONL and GCL thinning but without central chorioretinal atrophy in our study was otherwise normally laminated, arguing against a gross foveal maldevelopment.[28,29,50] The nearly circular areas of atrophy or parafoveal lesions involve a region characterized by steep, eccentricity-dependent changes in densities of ganglion cells and photoreceptors and their relative ratios.[22,51] The near circular appearance curiously matches the topography of the region with maximal retinal ganglion cell densities, cones adopting a less steep and more horizontally elongated density profile within this region.[51,52] Such early, well-demarcated foveal lesions are suggestive of a specific role of the vitamin B12 pathway in the maintenance and/or final development of this highly complex region.[28,29,40,44] The apparent normality of the RPE layer in the presence of ONL and GCL thinning at the youngest age examined in our series, and the emergence of RPE depigmentation and colocalized

Investigative Ophthalmology & Visual Science

parafoveal backscattering during follow-up, suggest that the RPE and choroidal changes may be secondary to photoreceptor loss, a testimony to the interdependence of photoreceptors, RPE, and choriocapillaris.[53]

There was retina-wide retinal degeneration in our older subjects, confirming previous observations and suggesting a different rate of progression in the extramacular retina. An interesting finding was the relative preservation (by NIR-REF and OCT) of the nasal peripapillary retina in some patients. The significance of this finding is unclear at this point, as we did not have enough documentation of the extramacular retina in sufficient numbers of patients to place this observation in a proper topographical context within the rest of the retina. Nevertheless, even older patients with retina-wide degeneration (e.g., P10 and P11) showed relative preservation of this region. Greater densities of cone photoreceptors and ganglion cells in normal extrafoveal nasal retina, particularly at 6 to 8 mm of eccentricity, compared to temporal retina may confer to the region a longer survival.[51] This horizontal asymmetry is less distinct at greater eccentricities, consistent with the reappearance of severe degeneration at greater eccentricities in nasal retina in our patients (Fig. 5A, P11; P10 in a previously published paper[8]).[51]

Laminopathy and Retinal Dysfunction in cblC-Associated Retinal Degeneration

An abnormally thickened INL in regions of total photoreceptor loss within the central retina and a thickened delaminated midperipheral inner retina in patients with retina-wide disease support a stereotypical remodeling response following photoreceptor degeneration.[8,30–32,36–39] Interestingly, the INL was within normal limits in younger patients with substantial ONL loss, a finding that was also apparent in OCT images in a recent report, perhaps evidence of a delay between the cellular death and the onset of the remodeling response.[22,54] There was slightly greater GCL than ONL loss in this study. The ganglion cell loss observed in a histologic report in cblC and in our patients could lead to transneuronal degeneration of photoreceptors and vice versa.[55] A normal INL in locations with prominent photoreceptor and ganglion cell loss argues against this possibility, assuming that our INL measurements are not underestimating neuronal loss within this layer.[32] Our finding favors a concurrent and perhaps independent neuronal loss in both retinal layers.

Replacement of optic nerve axons by nonneuronal elements has been associated with aging and glaucoma and seen as a remodeling response in hereditary retinal degenerations.[31,32,56,57] Retinal nerve fiber layer measured by SD-OCT in such a setting would underestimate true axonal loss and may explain the observation of normal or near-normal RNFL in the presence of severe GCL loss in the patients. The presence of a thickened hyperreflective band superficial to the GCL, particularly in peripapillary nasal retina, may represent a remodeling response or retinal maldevelopment.[39] Reports of developmental abnormalities in cblC disease are consistent with the latter.[2,6,14,58] The thickened superficial layer was observed when the GCL had thinned to between 60% to 80% of normal, with RNFL thinning occurring with greater GCL loss, favoring a remodeling sequence.[30–32,36–39] The precise interrelationships between each of the structural changes warrant further exploration in longitudinal studies to better understand the sequence of the retinal abnormalities in cblC.

There is evidence for a retina-wide, progressive, rod and cone photoreceptor dysfunction, and early photoreceptor loss has been documented by histopathology and by OCT in cblC.[8,14,16,18–20,22,23] Overall retinal function, however, was not affected initially by the metabolic abnormality, as evidenced by normal full-field ERGs in the presence of overt macular disease and metabolic derangement in our patients and in several previous reports.[8,18,21,22] Electroretinogram abnormalities reported in ~60% of patients with early-onset cblC disease likely represent spread of the disease beyond initially localized (foveal) lesions.[22] Changes in photoreceptor outer segment structure, now accessible to observation with SD-OCT and documented in cblC, may be the structural basis for the reported acute changes in photoreceptor function with improved metabolic control and may be used in the future as an additional gauge of treatment efficacy.[16,22]

With the exception of one patient who had normal vision and central retinal architecture associated with a milder metabolic phenotype, patients did not develop proper foveal function and had poor visual acuity and nystagmus even in the setting of a better-preserved foveal anatomy. Profoundly dysfunctional but anatomically preserved foveas occur in early-onset photoreceptor degenerations.[59,60] By comparison, the GCL abnormality observed in early-onset cblC adds a layer of complexity, as dysfunction may be occurring at different levels along the visual pathway. The role of amblyopia in this situation remains uninvestigated, but a structural–functional dissociation constitutes the proper scenario for the use of corrective treatments aimed to improve functioning and avert cell death.

Although the current treatment of cblC is less efficacious for early-onset disease, particularly for neurologic/cognitive and ocular manifestations, there is hope for improvement of the conventional management.[7,14,16,22,58,61–67] Our study suggests that early, more aggressive, or alternative managements should be pursued to prevent the long-term effects of early visual deprivation. Studies are also needed to further define if there is a relationship between the retinal structure and function and the neurologic and cognitive phenotype.[58,68] Such information could be used in conjunction with metabolic parameters to gauge and potentially improve the efficacy that therapeutic interventions may have on the neurologic, cognitive, and ocular health of these patients and, as a result, on their overall quality of life.

Acknowledgments

The authors thank Melissa Pham, Melissa Eihborn, Sonia Zhu, Jessica Barr, and Denise Pearson for their critical help.

Supported by grants from the National Institutes of Health Grant NEI-K12 EY-015398-10, Research to Prevent Blindness, Foundation Fighting Blindness, Hope for Vision, Macula Vision Research, Pennsylvania Lions Sight Conservation and Research Foundation, and the Research Foundation–Flanders (Belgium).

Disclosure: **L. Bonafede**, None; **C.H. Ficicioglu**, None; **L. Serrano**, None; **G. Han**, None; **J.I.W. Morgan**, None; **M.D. Mills**, None; **B.J. Forbes**, None; **S.L. Davidson**, None; **G. Binenbaum**, None; **P.B. Kaplan**, None; **C.W. Nichols**, None; **P. Verloo**, None; **B.P. Leroy**, None; **A.M. Maguire**, None; **T.S. Aleman**, None

References

1. Rosenblatt DS, Aspler AL, Shevell MI, Pletcher BA, Fenton WA, Seashore MR. Clinical heterogeneity and prognosis in combined methylmalonic aciduria and homocystinuria (cblC). *Inherit Metab Dis*. 1997;20:528–538.
2. Rosenblatt DS, Fenton WA. Inherited disorders of folate and cobalamin transport and metabolism. In: Scriver CR, Beaudet AF, Sly WS, Valle D, eds. *The Metabolic and Molecular Bases of Inherited Disease*. New York: McGraw-Hill; 2001:3897–3933.

3. Weisfeld-Adams JD, Morrissey MA, Kirmse BM, et al. Newborn screening and early biochemical follow-up in combined methylmalonic aciduria and homocystinuria, cblC type, and utility of methionine as a secondary screening analyte. *Mol Genet Metab*. 2010;99:116–123.
4. Lerner-Ellis JP, Tirone JC, Pawelek PD, et al. Identification of the gene responsible for methylmalonic aciduria and homocystinuria, cblC type. *Nat Genet*. 2006;38:93–100.
5. Morel CF, Lerner-Ellis JP, Rosenblatt DS. Combined methylmalonic aciduria and homocystinuria (cblC): phenotype-genotype correlations and ethnic-specific observations. *Mol Genet Metab*. 2006;88:315–321.
6. Nogueira C, Aiello C, Cerone R, et al. Spectrum of *MMACHC* mutations in Italian and Portuguese patients with combined methylmalonic aciduria and homocystinuria, cblC type. *Mol Genet Metab*. 2008;93:475–480.
7. Carrillo-Carrasco N, Sloan J, Valle D, Hamosh A, Venditti CP. Hydroxocobalamin dose escalation improves metabolic control in cblC. *J Inherit Metab Dis*. 2009;32:728–731.
8. Aleman TS, Brodie F, Garvin C, et al. Retinal structure in cobalamin C disease: mechanistic and therapeutic implications [published online ahead of print February 10, 2014]. *Ophthalmic Genet*. doi:10.3109/13816810.2014.885059.
9. Martinelli D, Deodato F, Dionisi-Vici C. Cobalamin C defect: natural history, pathophysiology, and treatment. *J Inherit Metab Dis*. 2011;34:127–135.
10. Mah W, Deme JC, Watkins D, et al. Subcellular location of MMACHC and MMADHC, two human proteins central to intracellular vitamin B12 metabolism. *Mol Genet Metab*. 2013;108:112–118.
11. Fofou-Caillierez MB, Mrabet NT, Chéry C, et al. Interaction between methionine synthase isoforms and MMACHC: characterization in cblG-variant, cblG and cblC inherited causes of megaloblastic anaemia. *Hum Mol Genet*. 2013;22:4591–4601.
12. Carmel R, Bedras AA, Mace JW, Goodman SI. Congenital methylmalonic aciduria-homocystinuria with megaloblastic anemia. Observations on response to hydroxycobalamin and on the effect of homocysteine and methionine on the deoxyuridine suppression test. *Blood*. 1980;55:570.
13. Cogan DG, Schulman J, Porter RJ, Mudd SH. Epileptiform ocular movements with methylmalonic aciduria and homocystinuria. *Am J Ophthalmol*. 1980;90:251–253.
14. Robb RM, Dowton SB, Fulton AB, Levy HL. Retinal degeneration in vitamin B12 disorder associated with methylmalonic aciduria and sulfur amino acid abnormalities. *Am J Ophthalmol*. 1984;97:691–696.
15. Mitchell GA, Watkins D, Melançon SB, et al. Clinical heterogeneity in cobalamin C variant of combined homocystinuria and methylmalonic aciduria. *J Pediatr*. 1986;108:410–415.
16. Tsina EK, Marsden DL, Hansen RM, Fulton AB. Maculopathy and retinal degeneration in cobalamin C methylmalonic aciduria and homocystinuria. *Arch Ophthalmol*. 2005;123:1143–1146.
17. Schimel AM, Mets MB. The natural history of retinal degeneration in association with cobalamin C (cblC) disease. *Ophthalmic Genet*. 2006;27:9–14.
18. Gerth C, Morel CF, Feigenbaum A, Levin AV. Ocular phenotype in patients with methylmalonic aciduria and homocystinuria, cobalamin C type. *J AAPOS*. 2008;12:591–596.
19. Fuchs LR, Robert M, Ingster-Moati I, et al. Ocular manifestations of cobalamin C type methylmalonic aciduria with homocystinuria. *J AAPOS*. 2012;16:370–375.
20. Gizicki R, Robert MC, Gomez-Lopez L, et al. Long-term visual outcome of methylmalonic aciduria and homocystinuria, cobalamin C type. *Ophthalmology*. 2014;121:381–386.
21. Collison FT, Xie YA, Gambin T, et al. Whole exome sequencing identifies an adult-onset case of methylmalonic aciduria and homocystinuria type C (cblC) with non-syndromic bull's eye maculopathy. *Ophthalmic Genet*. 2015;17:1–6.
22. Weisfeld-Adams JD, McCourt EA, Diaz GA, Oliver SC. Ocular disease in the cobalamin C defect: a review of the literature and a suggested framework for clinical surveillance. *Mol Genet Metab*. 2015;114:537–546.
23. Traboulsi EI, Silva JC, Geraghty MT, Maumenee IH, Valle D, Green WR. Ocular histopathologic characteristics of cobalamin C type vitamin B12 defect with methylmalonic aciduria and homocystinuria. *Am J Ophthalmol*. 1992;113:269–280.
24. Curcio CA, Messinger JD, Sloan KR, Mitra A, McGwin G, Spaide RF. Human chorioretinal layer thicknesses measured in macula-wide, high-resolution histologic sections. *Invest Ophthalmol Vis Sci*. 2011;52:3943–3954.
25. Marmor MF, Fulton AB, Holder GE, Miyake Y, Brigell M, Bach M. Standard for clinical electroretinography (2008 update). *Doc Ophthalmol*. 2009;118:69–77.
26. Huynh SC, Wang XY, Rochtchina E, Mitchell P. Distribution of macular thickness by optical coherence tomography: findings from a population-based study of 6-year-old children. *Invest Ophthalmol Vis Sci*. 2006;47:2351–2357.
27. Yanni SE, Wang J, Cheng CS, et al. Normative reference ranges for the retinal nerve fiber layer, macula, and retinal layer thicknesses in children. *Am J Ophthalmol*. 2013;155:354–360.
28. Vajzovic L, Hendrickson AE, O'Connell RV, et al. Maturation of the human fovea: correlation of spectral-domain optical coherence tomography findings with histology. *Am J Ophthalmol*. 2012;154:779–789.
29. Dubis AM, Costakos DM, Subramaniam CD, et al. Evaluation of normal human foveal development using optical coherence tomography and histologic examination. *Arch Ophthalmol*. 2012;130:1291–1300.
30. Huang WC, Cideciyan AV, Roman AJ, et al. Inner and outer retinal changes in retinal degenerations associated with *ABCA4* mutations. *Invest Ophthalmol Vis Sci*. 2014;55:1810–1822.
31. Aleman TS, Cideciyan AV, Sumaroka A, et al. Inner retinal abnormalities in X-linked retinitis pigmentosa with *RPGR* mutations. *Invest Ophthalmol Vis Sci*. 2007;48:4759–4765.
32. Aleman TS, Soumittra N, Cideciyan AV, et al. *CERKL* mutations cause an autosomal recessive cone-rod dystrophy with inner retinopathy. *Invest Ophthalmol Vis Sci*. 2009;50:5944–5954.
33. Cideciyan AV, Swider M, Aleman TS, et al. ABCA4 disease progression and a proposed strategy for gene therapy. *Hum Mol Genet*. 2009;18:931–941.
34. Knighton RW, Gregori G. The shape of the ganglion cell plus inner plexiform layers of the normal human macula. *Invest Ophthalmol Vis Sci*. 2012;53:7412–7420.
35. Drasdo N, Millican CL, Katholi CR, Curcio CA. The length of Henle fibers in the human retina and a model of ganglion receptive field density in the visual field. *Vision Res*. 2007;47:2901–2911.
36. Aleman TS, Cideciyan AV, Sumaroka A, et al. Retinal laminar architecture in human retinitis pigmentosa caused by Rhodopsin gene mutations. *Invest Ophthalmol Vis Sci*. 2008;49:1580–1590.
37. Jacobson SG, Cideciyan AV, Sumaroka A, et al. Remodeling of the human retina in choroideremia: rab escort protein 1 (*REP-1*) mutations. *Invest Ophthalmol Vis Sci*. 2006;47:4113–4120.
38. Jacobson SG, Sumaroka A, Aleman TS, Cideciyan AV, Danciger M, Farber DB. Evidence for retinal remodelling in retinitis pigmentosa caused by *PDE6B* mutation. *Br J Ophthalmol*. 2007;91:699–701.
39. Aleman TS, Cideciyan AV, Aguirre GK, et al. Human *CRB1*-associated retinal degeneration: comparison with the rd8 Crb1-mutant mouse model. *Invest Ophthalmol Vis Sci*. 2011;52:6898–6910.

Investigative Ophthalmology & Visual Science

40. Springer AD, Hendrickson AE. Development of the primate area of high acuity. 1. Use of finite element analysis models to identify mechanical variables affecting pit formation. *Vis Neurosci*. 2004;21:53–62.
41. Mazzoni F, Novelli E, Strettoi E. Retinal ganglion cells survive and maintain normal dendritic morphology in a mouse model of inherited photoreceptor degeneration. *J Neurosci*. 2008;28:14282–14292.
42. Heckenlively JR, Foxman SG, Parelhoff ES. Retinal dystrophy and macular coloboma. *Doc Ophthalmol*. 1988;68:257–271.
43. den Hollander AI, Roepman R, Koenekoop RK, Cremers FP. Leber congenital amaurosis: genes, proteins and disease mechanisms. *Prog Retin Eye Res*. 2008;27:391–419.
44. Verghese PB, Sasaki Y, Yang D, et al. Nicotinamide mononucleotide adenylyl transferase 1 protects against acute neurodegeneration in developing CNS by inhibiting excitotoxic-necrotic cell death. *Proc Natl Acad Sci U S A*. 2011;108:19054–19059.
45. Perrault I, Hanein S, Zanlonghi X, et al. Mutations in *NMNAT1* cause Leber congenital amaurosis with early-onset severe macular and optic atrophy. *Nat Genet*. 2012;44:975–977.
46. Koenekoop RK, Wang H, Majewski J, et al.; Finding of Rare Disease Genes (FORGE) Canada Consortium. Mutations in *NMNAT1* cause Leber congenital amaurosis and identify a new disease pathway for retinal degeneration. *Nat Genet*. 2012;44:1035–1039.
47. Falk MJ, Zhang Q, Nakamaru-Ogiso E, et al. *NMNAT1* mutations cause Leber congenital amaurosis. *Nat Genet*. 2012;44:1040–1045.
48. Chiang PW, Wang J, Chen Y, et al. Exome sequencing identifies *NMNAT1* mutations as a cause of Leber congenital amaurosis. *Nat Genet*. 2012;44:972–974.
49. Kaplan J, Perrault I, Hanein S, Dollfus H, Rozet JM. Mutations in *NMNAT1* cause Leber congenital amaurosis with severe macular and optic atrophy. *Med Sci (Paris)*. 2013;29:26–27.
50. Hendrickson A, Possin D, Vajzovic L, Toth CA. Histologic development of the human fovea from midgestation to maturity. *Am J Ophthalmol*. 2012;154:767–778.
51. Curcio CA, Allen KA. Topography of ganglion cells in human retina. *J Comp Neurol*. 1990;300:5–25.
52. Curcio CA, Sloan KR, Kalina RE, Hendrickson AE. Human photoreceptor topography. *J Comp Neurol*. 1990;292:497–523.
53. Fuhrmann S, Zou C, Levine EM. Retinal pigment epithelium development, plasticity, and tissue homeostasis. *Exp Eye Res*. 2014;123:141–150.
54. Jones BW, Watt CB, Frederick JM, et al. Retinal remodeling triggered by photoreceptor degenerations. *J Comp Neurol*. 2003;464:1–16.
55. Stone JL, Barlow WE, Humayun MS, de Juan E Jr, Milam AH. Morphometric analysis of macular photoreceptors and ganglion cells in retinas with retinitis pigmentosa. *Arch Ophthalmol*. 1992;110:1634–1639.
56. Quigley HA. Neuronal death in glaucoma. *Prog Retin Eye Res*. 1999;18:39–57.
57. Harwerth RS, Wheat JL. Modeling the effects of aging on retinal ganglion cell density and nerve fiber layer thickness. *Graefes Arch Clin Exp Ophthalmol*. 2008;246:305–314.
58. Weisfeld-Adams JD, Bender HA, Miley-Åkerstedt A, et al. Neurologic and neurodevelopmental phenotypes in young children with early-treated combined methylmalonic acidemia and homocystinuria, cobalamin C type. *Mol Genet Metab*. 2013;110:241–247.
59. Jacobson SG, Aleman TS, Cideciyan AV, et al. Defining the residual vision in Leber congenital amaurosis caused by *RPE65* mutations. *Invest Ophthalmol Vis Sci*. 2009;50:2368–2375.
60. Jacobson SG, Cideciyan AV, Peshenko IV, et al. Determining consequences of retinal membrane guanylyl cyclase (*RetGC1*) deficiency in human Leber congenital amaurosis en route to therapy: residual cone-photoreceptor vision correlates with biochemical properties of the mutants. *Hum Mol Genet*. 2013;22:168–183.
61. Enns GM, Barkovich AJ, Rosenblatt DS, et al. Progressive neurological deterioration and MRI changes in cblC methylmalonic acidaemia treated with hydroxocobalamin. *J Inherit Metab Dis*. 1999;22:599–607.
62. Bartholomew DW, Batshaw ML, Allen RH, et al. Therapeutic approaches to cobalamin-C methylmalonic acidemia and homocystinuria. *J Pediatr*. 1988;112:32–39.
63. Patton N, Beatty S, Lloyd IC, Wraith JE. Optic atrophy in association with cobalamin C (cblC) disease. *Ophthalmic Genet*. 2000;21:151–154.
64. Clarke C, Li M, Payan P, et al. Clinical, biochemical, molecular findings and outcomes of 8 children with cblC detected through newborn screening; 13 years experience. *J Inherit Metab Dis*. 2013;36(suppl 2):S314.
65. Matos IV, Castejón E, Meavilla S, et al. Clinical and biochemical outcome after hydroxocobalamin dose escalation in a series of patients with cobalamin C deficiency. *Mol Genet*. 2013;109:360–365.
66. Andersson HC, Marble M, Shapira E. Long-term outcome in treated combined methylmalonic acidemia and homocystinemia. *Genet Med*. 1999;1:146–150.
67. Richard E, Jorge-Finnigan A, Garcia-Villoria J, et al.; MMACHC Working Group. Genetic and cellular studies of oxidative stress in methylmalonic aciduria (MMA) cobalamin deficiency type C (cblC) with homocystinuria (MMACHC). *Hum Mutat*. 2009;30:1558–1566.
68. Fischer S, Huemer M, Baumgartner M, et al. Clinical presentation and outcome in a series of 88 patients with the cblC defect. *J Inherit Metab Dis*. 2014;37:831–840.

Investigative Ophthalmology & Visual Science